

Rotating neutron stars with non-barotropic thermal profile

Giovanni Camelio,¹ Tim Dietrich,² Miguel Marques, and Stephan Rosswog¹

¹*Department of Astronomy and The Oskar Klein Centre,
Stockholm University, AlbaNova, 10691 Stockholm, Sweden*

²*Nikhef, Science Park, 1098 XG Amsterdam, The Netherlands*

(Dated: November 13, 2019)

Neutron stars provide an excellent laboratory for physics under the most extreme conditions. Up to now, models of axisymmetric, stationary, differentially rotating neutron stars were constructed under the strong assumption of barotropy, where a one-to-one relation between all thermodynamic quantities exists. This implies that the specific angular momentum of a matter element depends only on its angular velocity. The physical conditions in the early stages of neutron stars, however, are determined by their violent birth processes, typically a supernova or in some cases the merger of two neutron stars, and detailed numerical models show that the resulting stars are by no means barotropic. Here, we construct models for stationary, differentially rotating, non-barotropic neutron stars, where the equation of state and the specific angular momentum depend on more than one independent variable. We show that the potential formulation of the relativistic Euler equation can be extended to the non-barotropic case, which, to the best of our knowledge, is a new result even for the Newtonian case. We implement the new method into the XNS code and construct equilibrium configurations for non-barotropic equations of state. We scrutinize the resulting configurations by evolving them dynamically with the numerical relativity code BAM, thereby demonstrating that the new method indeed produces stationary, differentially rotating, non-barotropic neutron star configurations.

I. INTRODUCTION

Black holes and neutron stars are the final stages of the evolution of massive stars, and they are typically born in supernova explosions or, less frequently, in binary neutron star mergers. Neutron stars are of particular interest since they allow for the study of matter properties under extreme density and temperature conditions that cannot be reached in any terrestrial laboratory, e.g., [1–5]. These matter properties, however, leave an imprint in the post-merger gravitational wave signal (at kHz frequencies) that will be accessible to ground-based gravitational wave detectors of the next generation, e.g. [6, 7]. Moreover, these properties impact also the post-merger neutrino and electromagnetic signals [8–11].

Stationary rotating equilibrium configurations are often used as idealizations of the post-merger remnant or as initial conditions for long-term evolutions and explorations of the parameter space [e.g., 12–16]. Thermal effects are in such studies included by assuming that all thermodynamical quantities, including the temperature, are functions of only one independent variable, e.g. the pressure. This leads to “effective barotropic” or simply “barotropic” stellar models which are particularly convenient because they allow to write the Euler equation as a potential.

The barotropic assumption is also commonly used to model Newtonian (e.g., main sequence) stars. In the context of Newtonian stars, however, non-barotropic stellar models (also called “baroclinic”) have been computed both perturbatively [17–20] and non-perturbatively [21–26], and even for Newtonian accretion disks with an analytic procedure [27, 28]. In a non-barotropic star, the thermodynamical quantities depend on more than one in-

dependent variable, for example on the pressure and the temperature, and the Euler equation needs to be solved numerically. While baroclinic stationary stars are known and studied in Newtonian theory, they have not yet been addressed in a General Relativity context¹. This is probably due by the difficulty of solving the Euler equation in differential form and the fact that thermal effects influence the neutron star structure only for the first few tens of seconds and are negligible thereafter.

Nevertheless, since post-merger and post-supernova remnants are not barotropic [e.g., 4, 5], or, more generally, since the lack of non-barotropic models in General Relativity represents a serious gap in the theory of stellar structure, we want to address this topic here. We address the non-barotropy of relativistic neutron stars, both theoretically and with stationary and dynamical numerical codes. The novelty of our work is twofold: on the one hand this is the first study in General Relativity of stationary, differentially rotating, non-barotropic stars; on the other hand we demonstrate that also in the non-barotropic case the Euler equation can be cast in the form of a potential. The latter result is novel even in the Newtonian context.

The paper is organized as follow. We discuss in Sec. II how thermal effects are commonly included in barotropic neutron star models. Sec. III describes our novel approach and its numerical implementation is explained in Sec. IV. The new approach is validated in Sec. V and Sec. VI discusses some of its implications. We finally

¹ Bardeen [29] explicitly considers a general entropy distribution in the formulation of his variational principle, but does not compute any stellar structure.

summarize and conclude in Sec. VII. In three appendices we describe the Newtonian limit of the (relativistic) Euler equation (Appendix A) and the non-barotropic (Appendix B) and the effective barotropic (Appendix C) equations of state adopted.

II. ROTATING STARS IN GENERAL RELATIVITY

Unless stated otherwise, we use $c = G = M_\odot = k_B = 1$, which are also our code units. Useful conversions to this unit system are $\text{km} \simeq 0.677$, $\text{ms} \simeq 203$, and $\rho_n \simeq 4.34 \times 10^{-4}$, where ρ_n is the nuclear saturation rest mass density ($\rho_n \simeq 2.68 \times 10^{14} \text{ g/cm}^3$).

In this work we are interested in solutions of stationary rotating stars in General Relativity. We will assume axisymmetry, since non-axisymmetric rotating bodies radiate gravitational waves and therefore are not stationary. We will further assume a circular spacetime, which implies the assumption that meridional currents and convection are negligible. Under these assumptions, the spacetime shaped by the rotating neutron star in quasi-isotropic coordinates reads [30]:

$$d\tau^2 = -\alpha^2 dt^2 + A^2(dr^2 + r^2 d\theta^2) + B^2 r^2 \sin^2 \theta (d\phi - \omega dt)^2, \quad (1)$$

where τ is the proper time, t, r, θ, ϕ are the coordinate time, radius, polar angle, and azimuth angle, respectively, and α, A, B, ω are metric fields that depend only on r, θ due to the stationarity and axisymmetry condition. α is the lapse and ω is the angular velocity of the zero angular momentum observer (ZAMO) as measured by an observer at infinity [29]. It is useful to define the cylindrical radius (which in General Relativity has not cylindrical isosurfaces):

$$R(r, \theta) = B(r, \theta) r \sin \theta. \quad (2)$$

With these assumptions, the Einstein equations reduce to four equations for the metric fields α, A, B, ω . Let us assume that the stellar matter is described by a perfect fluid, with energy-momentum tensor

$$T^{\mu\nu} = \mathcal{L} u^\mu u^\nu + p g^{\mu\nu}, \quad (3)$$

where u^μ is the 4-velocity, p is the pressure, and \mathcal{L} is the total enthalpy per volume. The Euler equation can be derived from the vanishing of the covariant divergence of the energy-momentum tensor as

$$\frac{\partial_i p}{\mathcal{L}} + \partial_i \ln \frac{\alpha}{\gamma} + F \partial_i \Omega = 0, \quad (4)$$

where $i = \{r, \theta\}$ [see Appendix A for the Newtonian limit of Eq. (4)]. γ and Ω are respectively the Lorentz factor with respect to the ZAMO and the matter angular speed

seen at infinity,

$$\gamma = \frac{1}{\sqrt{1 - (Rv^\phi)^2}}, \quad (5)$$

$$\Omega = \alpha v^\phi + \omega, \quad (6)$$

where v^ϕ is the contravariant matter 3-velocity with respect to the ZAMO, and F is:

$$F = u^t u_\phi = \frac{R^2(\Omega - \omega)}{\alpha^2 - R^2(\Omega - \omega)^2}. \quad (7)$$

The specific (per unit energy) angular momentum of a fluid element is given by

$$\ell = -\frac{u_\phi}{u_t} = \frac{R^2(\Omega - \omega)}{\alpha^2 + R^2\omega(\Omega - \omega)}, \quad (8)$$

which is equivalent to

$$F = \frac{\ell}{1 - \Omega \ell}. \quad (9)$$

Since for axisymmetry and stationarity $F = F(r, \theta)$, it follows that in general $\Omega = \Omega(r, \theta)$ and $\ell = \ell(r, \theta)$.

Stationary numerical solutions of the structure of relativistic rotating stars can be obtained by iteratively solving the metric and matter equations [30]. In the following sections, we will discuss the equations for matter fields. This means in particular that the metric fields α, A, B, ω are known and fixed from the previous iteration.

A. Isentropic EOS and rigid rotation

Considering an equation of state (EOS) depending on two variables with a thermal part, the first law of thermodynamics for the specific enthalpy reads

$$dh = \frac{dp}{\rho} + \frac{T}{m_n} ds, \quad (10)$$

where ρ is the rest-mass density, h the specific total enthalpy ($h = \mathcal{L}/\rho$), T is the temperature, m_n the nucleon mass, and s the entropy per baryon. Since one can get ρ and T from partial differentiation of h with respect to p and s ,

$$\frac{1}{\rho} = \left. \frac{\partial h}{\partial p} \right|_s, \quad (11)$$

$$T = m_n \left. \frac{\partial h}{\partial s} \right|_p, \quad (12)$$

it is natural to use the pair p, s as independent variables for the enthalpy and its derived quantities,

$$dh(p, s) = \frac{dp}{\rho(p, s)} + \frac{T(p, s)}{m_n} ds. \quad (13)$$

If the entropy is uniform in the star, then $ds = 0$ and² $h = h(p)$, namely the EOS is barotropic (i.e., 1D), and the first law of thermodynamics reads

$$d \ln h = \frac{dp}{\ell}. \quad (14)$$

In rigid rotation $\partial_i \Omega = 0$, and thanks to Eq. (14), we can write Eq. (4) as

$$\partial_i \ln h + \partial_i \ln \frac{\alpha}{\gamma} = 0, \quad (15)$$

which is equivalent to

$$\ln h(p) + \ln \frac{\alpha}{\gamma} = \text{const}, \quad (16)$$

where we can determine the constant from the known central values of the enthalpy h_0 and the lapse α_0 (on the axis $Rv^\phi = 0$ and therefore $\gamma = 1$):

$$\text{const} = \ln(h_0 \alpha_0). \quad (17)$$

From Eqs. (16)–(17) and fixing the uniform angular velocity $\Omega = \Omega_0$ one can easily get h and from it p and the other EOS quantities.

The most common example of neutron stars studied in the literature are cold stars (i.e., uniform vanishing entropy per baryon). An example of cold, rigidly rotating neutron star is marked as “CR” in this paper.

B. Barotropic EOS and differential rotation

Under the assumption that the entropy per baryon depends only on the pressure $s = \tilde{s}(p)$, a hot EOS depends on pressure alone, i.e. it becomes an effective barotrope:

$$h(p) = h(p, \tilde{s}(p)). \quad (18)$$

This can be observed in Fig. 1, where we show the entropy per baryon as a function of the rest-mass density in the interior of a neutron star. The black lines correspond to the effective barotropic assumption, while the red regions are obtained by dropping this assumption as described in Sec. III. It is convenient to define the “heat function”

$$H(p) = \int_{p_0}^p \frac{dp'}{\ell(p')}, \quad (19)$$

where p_0 is the given central pressure, from which we obtain

$$\partial_i H(p) = \frac{\partial_i p}{\ell}. \quad (20)$$

Additionally, if we assume that F depends only on Ω , we have analogously:

$$\mathcal{F}(\Omega) = \int_{\Omega_0}^{\Omega} F(\Omega') d\Omega', \quad (21)$$

$$\partial_i \mathcal{F}(\Omega) = F(\Omega) \partial_i \Omega, \quad (22)$$

where Ω_0 is the given angular frequency on the symmetry axis and $\mathcal{F}(\Omega)$ is called “differential-rotation law”. Using Eqs. (19)–(22), Eq. (4) is equivalent to

$$H(p) + \ln \frac{\alpha}{\gamma} + \mathcal{F}(\Omega) = \ln \alpha_0. \quad (23)$$

One can determine the matter properties in every point (r, θ) by determining Ω from the relation $\mathcal{F}'(\Omega) = F(\Omega, r, \theta)$, where we show explicitly the dependence on the yet-to-be-determined Ω , and then p from Eqs. (19) and (23). The other EOS quantities are easily determined because the EOS is effectively barotropic.

For an isentropic star it is $H(p) = \ln h(p) - \ln h_0$, and if in addition the star is in rigid rotation, one recovers Eq. (14), as expected.

One can assume an analytic form for the differential-rotation law, for example by adopting the “j-const” law that is commonly used in literature ([31], see also [32, 33]):

$$\mathcal{F}(\Omega) = -\frac{R_0^2}{2} (\Omega - \Omega_0)^2, \quad (24)$$

where R_0 has the dimension of a length and sets the scale of the differential rotation, that is, $\Omega \simeq \Omega_0/2$ at $R = R_0$ [34]. Rigid rotation cannot be described by a differential-rotation law because Ω is constant, but F is not. Therefore, it can only be recovered in the limit $R_0 \rightarrow \infty$. To model rigid rotation, one can just fix $\Omega = \Omega_0$ and drop the \mathcal{F} term in Eq. (23); however in Sec. VID we show how it is possible to cleanly unify the description of rigidly and differentially rotating stars.

The assumption $F = F(\Omega)$ is equivalent to requiring that $\ell = \ell(\Omega)$ [cf. Eq. (9)], namely it is equivalent to dropping any dependence on the metric and the coordinates in the relation between the specific angular momentum and the angular speed. This can be seen in Fig 2, where we show the specific angular momentum as a function of the angular velocity in the interior of a neutron star. The black line corresponds to the case discussed in this section, where the specific angular momentum is in a one-to-one correspondence with the angular velocity, while the red region is obtained by dropping this assumption as described in Sec. III.

III. NON-BAROTROPIC THERMAL PROFILE

The big problem of the method described in the previous section is that one is limited to an effective barotropic

² For simplicity we use in this work the same symbol for functions that represent the same physical quantity but depend on different independent variables, even if mathematically they differ since they are defined on different domains. We will always specify the independent variables if they are not clear from the context.

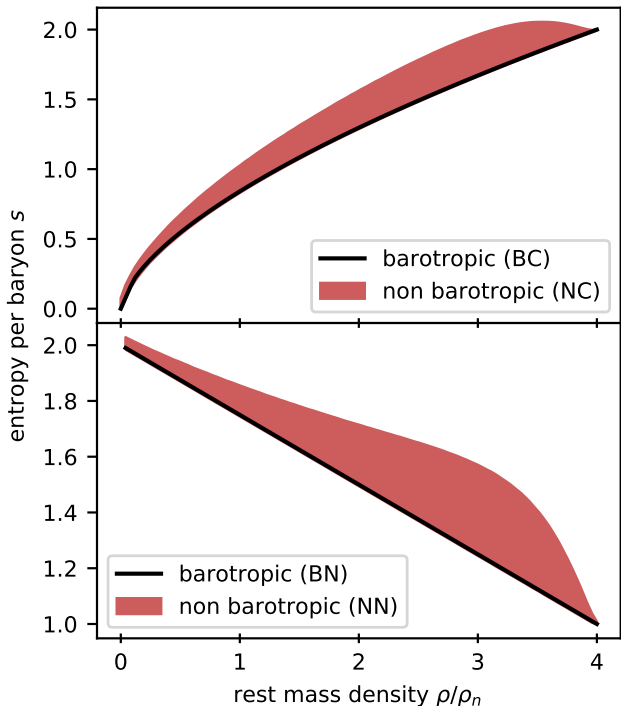


FIG. 1: Entropy per baryon s as a function of rest-mass density ρ for 2 barotropic (black lines) and 2 non-barotropic (red regions) models considered in this paper, cf. Table I. The upper/lower edge of the red regions corresponds to the entropy along the equatorial plane/rotational axis of the non-barotropic neutron star, respectively. Similar plots obtained from dynamical simulations are e.g. Fig. 1 of Fischer et al. [5] and Figs. 3–8 of Perego et al. [4].

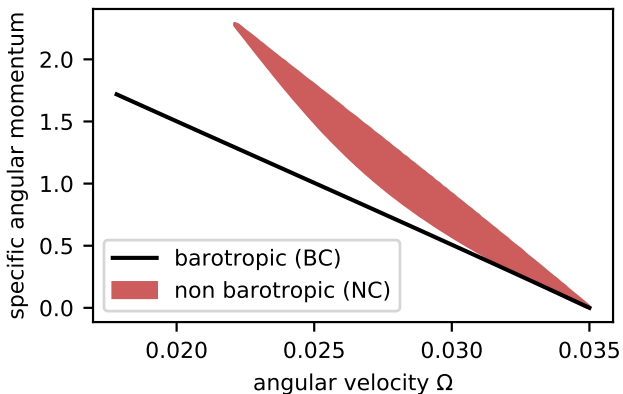


FIG. 2: Angular momentum per unit energy ℓ as a function of angular velocity Ω for a barotropic (black line) and a non-barotropic (red region) model considered in this paper, cf. Tab. I. The upper/lower edge of the red region corresponds to the specific angular momentum along the equatorial plane/stellar border, respectively. Non-convective models behave similarly.

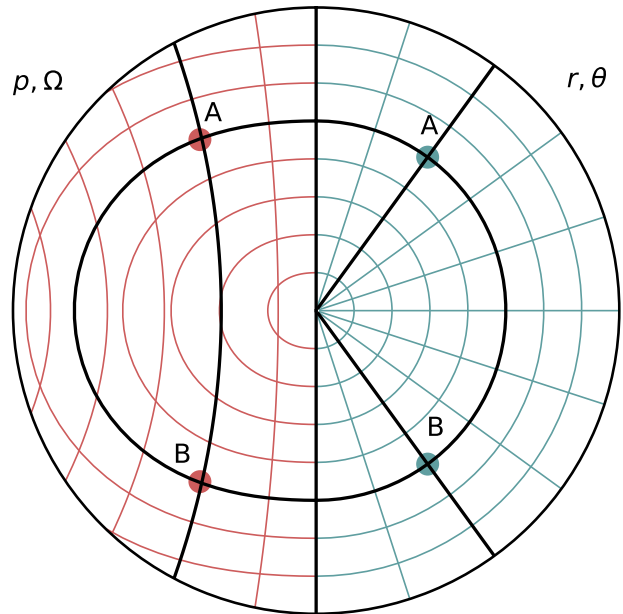


FIG. 3: Sketch of the coordinate grid in p, Ω (left, red) and in r, θ (right, blue). The p coordinate is elliptic-like while the Ω coordinate is parabolic-like, cf. Fig. 6. Note that the planar symmetric A and B points have different θ coordinate but the same p, Ω coordinates.

EOS, i.e. the EOS is actually a function of one independent variable only, even in presence of thermal effects. Similarly, one enforces $\ell = \ell(\Omega)$, dropping any dependence on the metric, see black lines in Figs. 1 and 2. However, dynamical core-collapse supernova and binary neutron star merger simulations show that realistic newly-born neutron stars are non-barotropic [e.g., 4, 5].

In this section we show how it is possible to overcome these limitations in a rigorous way.

A. The generalization

Eq. (4) can be written as

$$\frac{dp}{\ell} + F d\Omega + d \ln \frac{\alpha}{\gamma} = 0, \quad (25)$$

to stress that when $\ell = \ell(p)$ and $F = F(\Omega)$ it is

$$d \left(H(p) + \mathcal{F}(\Omega) + \ln \frac{\alpha}{\gamma} \right) = 0, \quad (26)$$

namely the Euler equation implies the existence of a conserved quantity and

$$\frac{1}{\ell} = \frac{dH(p)}{dp}, \quad (27)$$

$$F = \frac{d\mathcal{F}(\Omega)}{d\Omega}. \quad (28)$$

In other words, we are casting the Euler equation in a potential form similar to Thermodynamics. However, comparing the thermodynamical case [e.g., Eqs. (11)–(12)] with the stellar case [i.e., Eqs. (27)–(28)], one notes that in contrast to the former, in the latter we are determining the derived quantities with total derivatives of two potentials instead of partial derivatives of one potential. *Here we push the similarity with Thermodynamics one step further.*

Let us pursue this intuition:

$$Q(p, \Omega) = -\ln \frac{\alpha}{\gamma}, \quad (29)$$

$$\partial_i Q(p, \Omega) = \frac{\partial_i p}{\mathcal{L}(p, \Omega)} + F(p, \Omega) \partial_i \Omega, \quad (30)$$

$$\frac{1}{\mathcal{L}(p, \Omega)} = \left. \frac{\partial Q(p, \Omega)}{\partial p} \right|_{\Omega}, \quad (31)$$

$$F(p, \Omega) = \left. \frac{\partial Q(p, \Omega)}{\partial \Omega} \right|_p, \quad (32)$$

where we defined the potential Q and all quantities depend on p, Ω because these are the natural variables for the same reason p and s are the natural variables for the thermodynamical case, namely because the other quantities (\mathcal{L} and F in the stellar case, ρ and T in the thermodynamical case) can be determined from partial differentiation with respect to those. Note that Eq. (30) is exactly the Euler equation [Eq. (4)] and that it mirrors the equivalent thermodynamical equation [after substituting the exact differential with partial differentiation in Eq. (13)].

We should be careful because for axisymmetry and stationarity it is also $Q = Q(r, \theta)$, $p = p(r, \theta)$, and $F = F(r, \theta)$: given the pair p and Ω , we must be able to determine the pair r and θ . However, this change of coordinates is not bijective, that is, each pair p and Ω corresponds to two pairs r and θ , one in the northern hemisphere and one in the southern hemisphere, and therefore to two potentials: $Q_+(p, \Omega)$ and $Q_-(p, \Omega)$, that are identical in the planar case $Q_+ = Q_-$. In Fig. 3 we show how the interior of a star is mapped with r and θ coordinates (on the right) and with p and Ω coordinates (on the left).

The key point here is that the additional dependence of \mathcal{L} on Ω [as opposed to a dependence only on p , see Eq. (31)] “breaks” the barotropicity because, as can be seen in Fig. 3, Ω is not in a one-to-one correspondence with p . This additional dependence is made possible by allowing for $\partial_p \partial_{\Omega} Q \neq 0$.

It is worth noting that:

- The standard case described in Sec. II B is equivalent to the following potential:

$$Q(p, \Omega) = H(p) + \mathcal{F}(\Omega) - \ln \alpha_0. \quad (33)$$

- Since we rewrote Eq. (4) in terms of a potential, the difference of pressure and angular speed between two stellar points does not depend on the

integration path but only on the initial and final points.

- From the Schwarz’s theorem we get the Maxwell-like relation

$$\left. \frac{\partial \mathcal{L}^{-1}}{\partial \Omega} \right|_p = \left. \frac{\partial F}{\partial p} \right|_{\Omega}. \quad (34)$$

B. A simple non-barotropic model

Assuming that the analytic form of $Q(p, \Omega)$ is known, but that we do not know the pressure and angular velocity profiles $p(r, \theta)$ and $\Omega(r, \theta)$, we have to solve the following system of equations in every point:

$$Q(p, \Omega) = -\ln \frac{\alpha(r, \theta)}{\gamma(r, \theta, \Omega)}, \quad (35)$$

$$\partial_{\Omega} Q(p, \Omega) = F(r, \theta, \Omega), \quad (36)$$

$$\partial_p Q(p, \Omega) = \frac{1}{\mathcal{L}(p, s(r, \theta))}. \quad (37)$$

In Eqs. (35)–(37) we have made explicit the dependence of every quantity on the position in the star (r, θ) and on the yet-to-be-determined quantities (p, Ω) . Given a point in the star (r, θ) and the entropy in that point $s(r, \theta)$, this is a system of 3 equations in 2 variables (p, Ω) , that in general has no solution. On the other hand, if we leave $s(r, \theta)$ undetermined, given (r, θ) we can first determine (p, Ω) solving Eqs. (35)–(36), and then determine $s(r, \theta)$ from Eq. (37).

Let us now consider a simple³ non-trivial case:

$$Q(p, \Omega) = Q_0 + H(p) + \mathcal{F}(\Omega) + bH(p)\mathcal{F}(\Omega), \quad (38)$$

where b is a “barotropic” parameter and the constant Q_0 is determined from the condition $Q_0 = Q(p_0, \Omega_0) = -\ln \alpha_0$. The standard case of Eq. (33) is re-obtained for $b = 0$. H and \mathcal{F} are formally defined as in Eqs. (19) and (21), but have not the same physical meaning. In particular, the arbitrary barotropic function $\tilde{s}(p)$ that enters in the definition of $H(p)$ does not correspond to a physical entropy unless $b = 0$ (this is the reason we defined it with a tilde).

The potential Q in this form is particularly convenient, because we can factor out the dependence on p and therefore we have to solve only one equation to determine Ω . In fact, Eq. (36) reads

$$\mathcal{F}'(\Omega)(1 + bH(p)) = F(r, \theta, \Omega), \quad (39)$$

³ Note that this is not the only potential that generalizes the standard case; for example another valid choice is obtained by substituting $Q_0 \rightarrow 0$ and $H(p) \rightarrow H(p) - \ln \alpha_0$ in Eq. (38), which gives a different but still consistent solution.

and using the definition (38) we get

$$\begin{aligned} \mathcal{F}'(\Omega)(1 + bQ(r, \theta, \Omega) - bQ_0) \\ = F(r, \theta, \Omega)(1 + b\mathcal{F}(\Omega)), \end{aligned} \quad (40)$$

that can be solved for Ω with a 1D root finding [$Q(r, \theta, \Omega)$ is the RHS of Eq. (35)]. Knowing Ω , one can first determine $H(p)$ and then ℓ from

$$H(p) = \frac{Q(r, \theta, \Omega) - Q_0 - \mathcal{F}(\Omega)}{1 + b\mathcal{F}(\Omega)}, \quad (41)$$

$$\ell(p, \Omega) = \frac{1}{H'(p)(1 + b\mathcal{F}(\Omega))}, \quad (42)$$

where $H'(p)$ is the total derivative of $H(p)$. Knowing ℓ and p [obtained from the inversion of $H(p)$] one can use them to invert the EOS, that in the case considered here depends on two independent variables (we discuss in Sec. VIC how to generalize the procedure to an EOS that depends on more than two independent variables).

It is useful at this point to recap what we have accomplished. We have first defined in Eq. (38) a function $Q(p, \Omega)$ and then enforced with Eqs. (35)–(37) that this function acts as a potential for the Euler equation. In this way both the matter and the rotational profiles of the star are uniquely determined from the potential Q and are function in general of more than one independent variable, therefore breaking the stellar barotropicity. In Sec. VIB we show how, in principle, one can use the freedom in the definition of Q to tune the thermodynamical and rotational profiles.

Note that for the non-barotropic models in Figs. 1 and 2 (red filled contours) the relations $s = s(\rho)$ and $\ell = \ell(\Omega)$ do not hold anymore.

IV. NUMERICAL IMPLEMENTATION

A. XNS code

The XNSv2 code [14, 15] determines the stationary structure of a rotating neutron star in the eXtended Conformal Flatness Condition (XCFC) approximation [35]. The metric equations are solved with a spherical harmonics decomposition on the angular direction and with finite differences along the radial direction. In the XCFC approximation the metric equations are simpler and hierarchically decoupled; this approximation is equivalent to enforce in Eq. (1)

$$A(r, \theta) \equiv B(r, \theta) \equiv \psi^2(r, \theta), \quad (43)$$

where ψ is called conformal factor, and it is justified because the maximal relative difference between the A and B metric functions is of the order of 10^{-3} [36]. The XCFC approximation yields results of excellent accuracy for rotating neutron stars [e.g., 16], while has been showed to

degrade for differentially rotating neutron stars [37]. Using the diagnostic formula of Eq. (20) of Iosif and Stergioulas [37], we estimate for the configurations studied in this paper a maximal error for local quantities (e.g., the angular velocity at the equator) within 2% and a much smaller error for global quantities (e.g., the gravitational mass). The estimated error is adequate for a good description of the rotating neutron star and its spacetime. In any case, we emphasize that the non-barotropic theory, which we develop in this paper, does not depend in any way on the use of the XCFC approximation.

In this paper we use our modified version [16] of XNSv2 and simply refer to it as XNS in the following. In Camellio et al. [16] we described and validated it against the RNS code [38] that solves the stationary configuration of rotating neutron stars in general relativity without approximations. We refer the reader to [14–16, 35] for the general structure of XNS and the XCFC equations and just describe the main modifications with respect to [16].

To determine the solution of a rotating star, XNS iterates between the solution of the metric and the matter equations until convergence. When the matter quantities (ℓ, p, v^ϕ) are updated, the metric quantities (α, ψ, ω) are kept fixed, and vice versa. To update the matter quantities, the following procedure is repeated for each grid point r_i, θ_j (we start from the center, $r_i = r_1$, and increase i outward):

1. If the star is rigidly rotating, set $\Omega = \Omega_0$. Otherwise, determine Ω from Eq. (40).
2. Find $H(p)$ from Eq. (41).
3. Find p inverting $H(p)$.
4. If $p < p_s$ (p_s being a fixed value of the surface pressure), go to step 8.
5. If the star is non-barotropic:
 - (a) Find ℓ from Eq. (42).
 - (b) If the pair ℓ, p is not physical (e.g., $\ell \leq p$), go to step 8.
6. All independent quantities have been computed. Solve the EOS from p (if barotropic) or p, ℓ (if non barotropic). Determine v^ϕ from Ω .
7. Go to step 1 with the next r_i .
8. The point is outside the surface. Set to zero all matter quantities in $r \geq r_i$ and go to step 1 with $r_i = r_1$ and the next θ_j .

We adopt a rectangular non-evenly spaced grid in r, θ [16]. Our radial grid is divided in two regions: the inner part has 2000 evenly spaced points from $r = 0$ excluded to $r = 15$ and the outer part has 2000 increasingly spaced points from $r = 15$ to $r = 1000$. The angular grid ($0 < \theta < \pi$) contains 501 points on the Legendre knots. We used 50 angular harmonics in the pseudo-spectral expansion and we consider the result converged

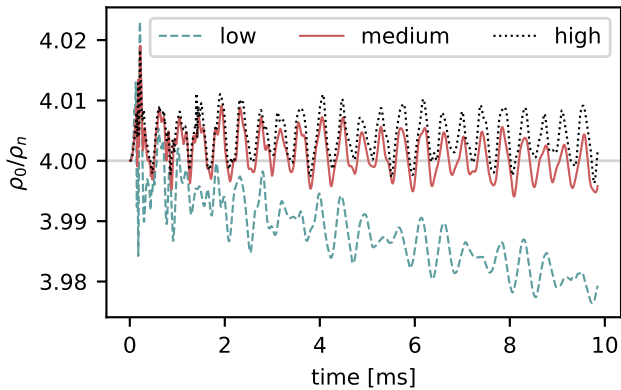


FIG. 4: BAM evolution of the central rest-mass density of the stellar model CR for different resolutions.

when the maximal absolute variation of the rest-mass density between two iterations is smaller than 10^{-12} . The surface pressure is set to $p_s = 10^{-40}$ in code units ($c = G = M_\odot = 1$).

B. BAM code

We also study the dynamical evolution of the XNS configurations with the BAM code [39–44]. BAM employs a simple mesh refinement scheme where the grid is composed of nested Cartesian boxes. The grid setup is controlled by the resolution Δx in the finest levels. The outer levels are constructed by progressively coarsening the resolution by factors of two. We solve the Einstein Equations using the Z4c evolution scheme [45–47] and employ fourth order finite-difference stencils. The equations of general relativistic hydrodynamics employ a finite-volume shock-capturing method and the hydrodynamical flux is computed with the Local Lax-Friedrichs scheme using the WENOZ limiter [43, 48].

The evolution equation system is closed with the EOS, for which we assume an ideal gas with a cold and a thermal contribution:

$$p(\rho, u_{\text{th}}) = K\rho^\Gamma + (\Gamma_{\text{th}} - 1)\rho u_{\text{th}}, \quad (44)$$

where u_{th} is the specific thermal energy and $K, \Gamma, \Gamma_{\text{th}}$ are EOS-dependent parameters, cf. Appendix B and Tables I and II.

To proof the robustness of our numerical scheme, we show the central rest-mass density evolution of the CR model, i.e., of a cold, rigid rotating neutron star, in Fig. 4; we refer the interested reader to [42, 43, 49–51] for additional tests and convergence analyses.

We increase the BAM resolution by factors of two, where for the low resolution (blue line) the minimum grid resolution in the finest level is 0.1875, the medium resolution (red line) has a minimum grid spacing of 0.09375, and the high resolution (black line) has a minimum grid

name	configuration
CR	Cold, Rigidly rotating
BC	differentially rotating, Barotropic, Convective
NC	differentially rotating, Non-barotropic, Convective
C Ω	Control with $b = 0$ in Eq. (40)
C p	Control with $b = 0$ in Eq. (42)
BN	differentially rotating, Barotropic, Non-convective
NN	differentially rotating, Non-barotropic, Non-convective

TABLE I: Abbreviated names of the stellar configuration studied in this work.

spacing of 0.046875. This is compatible to the highest resolved binary neutron star simulations performed for gravitational wave model development to date [52, 53]. We save computational costs by simulating only a single quadrant of the numerical domain making use of the axisymmetry of the spacetime and the planar symmetry of the models. From Fig. 4, we conclude that the changes in the central density decrease with increasing resolution. In particular, the central density decrease, which is present in the low resolution case, is small for the medium and high resolution. The remaining density oscillations of the order of $\sim 0.25\%$ seems negligible for the studies discussed in the following⁴. If not otherwise stated, we will show the results for the high resolution grid configuration, but all models have been simulated with the low, medium, and high grid resolutions to test the correctness of our results.

C. Models

To minimize additional code changes in BAM and XNS, we use throughout this work an EOS such that the total energy density is given by

$$\epsilon(\rho, s) = \rho + k_1\rho^\Gamma + k_2s^2\rho^{\Gamma_{\text{th}}}, \quad (45)$$

where $k_1, k_2, \Gamma, \Gamma_{\text{th}}$ are parameters specified in Table II. With our parameter choice this EOS has a maximal cold, non-rotating neutron star mass of $2.22 M_\odot$ as shown in Fig. 5, and can be straightforwardly included in BAM, since it is equivalent to an ideal gas EOS with $K = (\Gamma - 1)k_1$ (Appendix B).

We fix the barotropic function by setting $\tilde{s}(\tilde{\rho})$. We remark that with our choice of the potential Q , $\tilde{\rho}$ and \tilde{s} are physical rest-mass density and entropy per baryon also when $b \neq 0$ only on the rotational axis, since there

⁴ We remark that the remaining density oscillations is likely to be related to the XCFC approximation of XNS, since it is absent or smaller if the XCFC approximation is not employed; cf. Fig. 2 of [43] for single star evolutions and the supplementary material of [51] for studies in binary neutron star configurations.

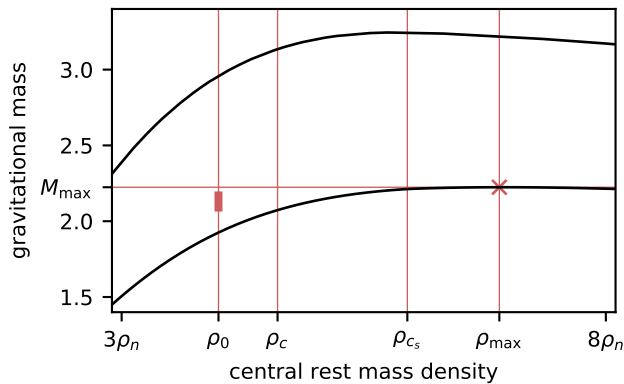


FIG. 5: Gravitational mass as a function of the central density for the EOS adopted in this paper with causality enforced at $\rho > \rho_{cs} = 5.95\rho_n$. The lower black line corresponds to non-rotating cold models and the upper black line to cold models that rotate rigidly at the Keplerian limit. $M_{\max} = 2.22$ is the maximal non-rotating mass corresponding to $\rho_{\max} = 6.90\rho_n$ (red cross) and $\rho_c = 4.60\rho_n$ is the critical density for inverting the non-barotropic EOS (see Appendix B). The thick red line marks the region of central density and gravitational (Komar) mass of the models considered in this paper ($\rho_0 = 4\rho_n$).

$\mathcal{F}(\Omega_0) = 0$. For this reason, there is no ambiguity in using the central quantities in Table II.

We consider 7 models, all shown in Fig. 6 and described in Tables I and II. We remark that if two quantities have parallel level contours means that they are in a one-to-one correspondence, cf. Fig. 6. The control configurations $C\Omega$ and Cp have been obtained with the same procedure as NC, but for $C\Omega$ we set $b = 0$ in Eq. (40) and for Cp we set $b = 0$ in Eq. (42). For this reason, $\ell = \ell(\Omega)$ for $C\Omega$ and $s = s(p)$ for Cp . Since the potential Q has not been solved consistently, $C\Omega$ and Cp are expected not to be true stationary solutions and are therefore our control models against which we will judge the quality of the theory.

The parameters of the EOS and of the potential Q that completely determine the stellar models are shown in Table II. The values of parameters R_0 and b have been chosen to emphasize differential rotation and non-barotropicity, while the choice of the other parameter values is discussed in Appendix B. All models are stable against dynamical instabilities, i.e., they do not collapse (Appendix B), but some models are unstable against convection (Appendix C). Note that the obtained central temperatures T_0 are reasonable for proto-neutron stars and for post-merged neutron stars.

More details on the EOS and the rationale behind our choices are provided in Appendices B and C.

V. RESULTS

A. Test 1: barotropic limit

We checked that, using the non-barotropic inversion of the EOS (namely steps 5.a–5.b in Sec. IV A), we obtain the same stationary results for the cold, rigid rotating model CR (having drop the \mathcal{F} term) and for the barotropic, differentially rotating models BC and BN.

B. Test 2: first integral residual

We define the residuals of the Euler equation as

$$\delta_i(r, \theta) = \partial_i Q(r, \theta) - \frac{\partial_i p(r, \theta)}{\mathcal{L}(r, \theta)} - F(r, \theta) \partial_i \Omega(r, \theta), \quad (46)$$

where $i = r, \theta$ is the direction of differentiation. To quantify how well Eq. (4) is solved in the star we use the averaged logarithm of the residuals:

$$\langle \log |\delta_i| \rangle = \frac{\sum_j \log_{10} |\delta_i(r_j, \theta_j)|}{N}, \quad (47)$$

where j is the index that identifies a point inside the star and N is the total number of points inside the star. These quantities should be compared with the potential Q which is in the range $0.3 \lesssim Q \lesssim 0.8$. We report the residuals in Table II. As expected, the Euler equation has in average a much worse residual (2-3 orders of magnitude) in the control configurations than in the consistently determined ones, thus corroborating our theory.

C. Test 3: stellar oscillations

As a final check, we evolved the XNS models with BAM to see whether the configurations are indeed in equilibrium. In particular, we want to compare the amplitude of the oscillations that are artificially triggered by numerical inaccuracies and by the use of the XCFC approximation for the initial setup. In Fig. 7 we show the central rest mass density evolution, and in Fig. 8 we compare the initial configuration with a snapshot close to the maximum of the final oscillation (marked with crosses in Fig. 7), in such a way to maximize deviations. Indeed, control configurations diverge much more than the consistently determined ones.

However, as discussed in Appendix C, models BC and NC are unstable against convection (note the convective patterns in the velocity field for these configurations in Fig. 8). Moreover, the convective timescale is comparable with the evolution time (Appendix C), and therefore also these consistently determined stellar configurations deviate from the initial ones.

We thus evolved 2 models that are stable against convection, BN and NN. These configurations have small oscillations comparable to that of the cold rigidly rotating model CR, thus verifying our theory.

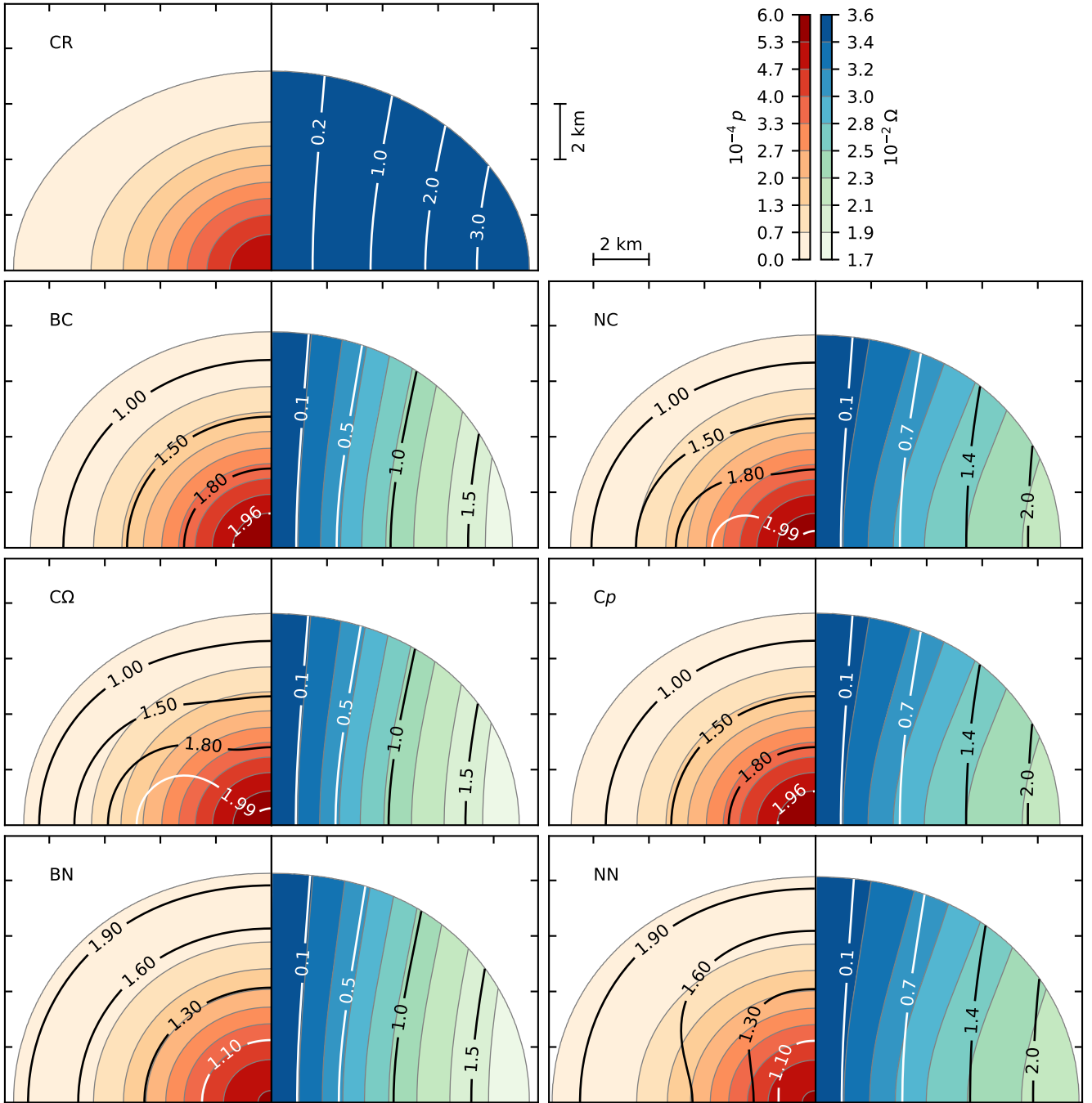


FIG. 6: Stationary stellar models obtained with XNS. For each model, the color filled contours refer to the pressure p (red scale, left) and the angular velocity Ω (blue scale, right), while the thick black and white contours to the entropy per baryon s (left) and the specific angular momentum ℓ (right). See text for details.

In Fig. 9 we compare the evolution of the non-barotropic setup for the convective and non-convective star. Convection begins at the stellar surface, where the convective timescale is shorter (Appendix C), and propagates to the interior, destroying the non-barotropic pattern and flattening the entropy profile. We have also simulated the evolution of a low resolution NC setup for a

much longer time. This low resolution simulation reproduces the qualitative patterns of the high resolution one and in it the convective cells disappear after $t \simeq 10$ ms, in line with the qualitative estimates of the convective

name	Γ	k_1	K	Γ_{th}	k_2	ρ_0	$\tilde{s}(\tilde{\rho})$	Ω_0	R_0	b	M	$\langle \log \delta_r \rangle$	$\langle \log \delta_\theta \rangle$	T_0 [MeV/k _B]
CR	3	5×10^4	10^5	1.75	1.5	$4\rho_n$	0	0.035	∞	0	2.17	-7.0	-7.6	0
BC	"	"	"	"	"	"	$2(\tilde{\rho}/\rho_0)^{5/8}$	"	15 km	0	2.12	-7.0	-7.4	48
NC	"	"	"	"	"	"	"	"	"	-2	2.15	-7.0	-7.4	"
$C\Omega$	"	"	"	"	"	"	"	"	"	-2*	2.16	-4.2	-4.1	"
Cp	"	"	"	"	"	"	"	"	"	-2*	2.15	-4.6	-5.6	"
BN	"	"	"	"	"	"	$2 - \tilde{\rho}/\rho_0$	"	"	0	2.09	-7.0	-7.2	24
NN	"	"	"	"	"	"	"	"	"	-2	2.12	-6.9	-7.1	"

TABLE II: Parameters and properties of the stellar models considered in this work. The first column is the name of the model (see Sec. IV C), columns 2–6 are the EOS parameters, columns 7–11 are the parameters of the potential Q , and columns 12–15 are model properties. Symbol ‘ ’ means “same as above” and the asterisk means that b was included in a non-consistent way in $C\Omega$ and Cp . See text for details.

timescale made in Appendix C⁵.

As final remarks, we point out that:

- The control models too are unstable against convection; however the non-consistency of the initial configurations has a much larger destabilizing effect, cf. Fig. 7.
- It is possible to obtain equilibrium models of neutron stars that are unstable against convection as it is possible to obtain equilibrium models that are dynamically unstable (i.e., that collapse [16]).

VI. DISCUSSION

A. Consequences

In the following we list some general results that can be directly derived with our novel approach:

1. The Schwarz’s theorem implies that if $F = F(\Omega)$, then $s = s(p)$, namely the EOS is an effective barotrope. The vice versa is also true.
2. The Schwarz’s theorem implies that a stationary neutron star with a non-barotropic thermal profile must also be differentially rotating.
3. On the symmetry axis F vanishes; then if the star is barotropic [namely $\Omega = \Omega(F)$] the angular velocity is uniform on the symmetry axis. However, this is not true in general for a non-barotropic star (but it is for the non-barotropic cases considered in this work) [18, 19, 21, 23, 24, 26].

⁵ We note the larger entropy at the star’s surface for the low resolution NC model. This entropy production is caused by the surface as discussed, e.g., in Guercilena et al. [54]. The entropy production decreases with an increasing resolution and its origin lies in the high-resolution shock-capturing schemes and the use of an artificial atmosphere surrounding the star.

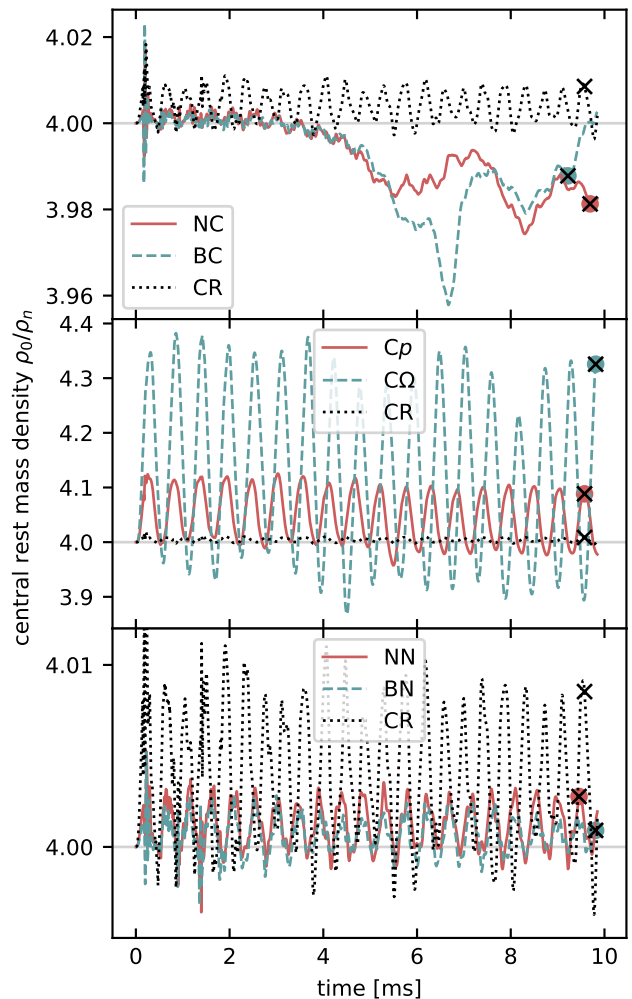


FIG. 7: Time dependence of the central rest mass density in the BAM evolution for the models considered in this paper. The cold, rigidly rotating model CR is plotted in all panels as reference. The crosses mark the snapshots shown in Fig. 8 and the gray horizontal lines mark the initial central density.

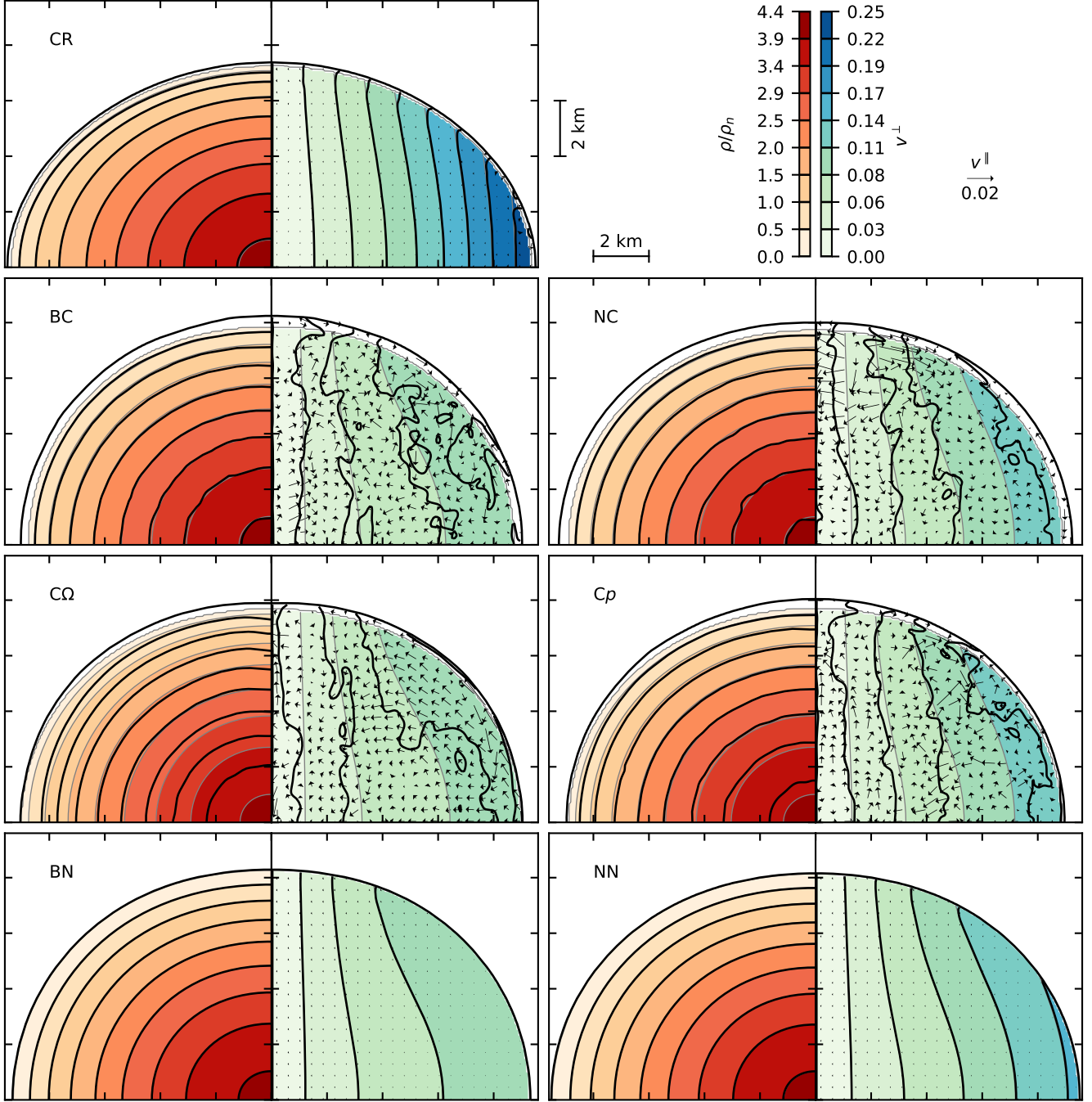


FIG. 8: BAM evolution. For each model, we plot the density ρ (red scale, left) and the orthogonal velocity $v^\perp = r \sin(\theta)v^\phi$ (blue scale, right). The initial configurations are shown in color filled contours delimited by thin gray contours while the configurations marked in Fig. 7 are shown in black thick contours with the parallel velocity $v^\parallel = v^r \mathbf{e}_r + rv^\theta \mathbf{e}_\theta$ shown as a vector field. Any deviance from stationarity during the evolution is due to convection and/or to the non consistency of the initial setup. See text for details.

4. An interesting point that emerges from Sec. III is that there are only two EOS quantities that can be directly determined from the Euler equation without solving the EOS, namely p and ℓ . This should not be a surprise because p and ℓ are the only

EOS quantities that appear in the definition of the energy-momentum tensor, Eq. (3). When other quantities like $\ln h$ and s appear in the equations, they correspond to physical quantities only in some limits, e.g., for isentropic stars in the case of $\ln h$

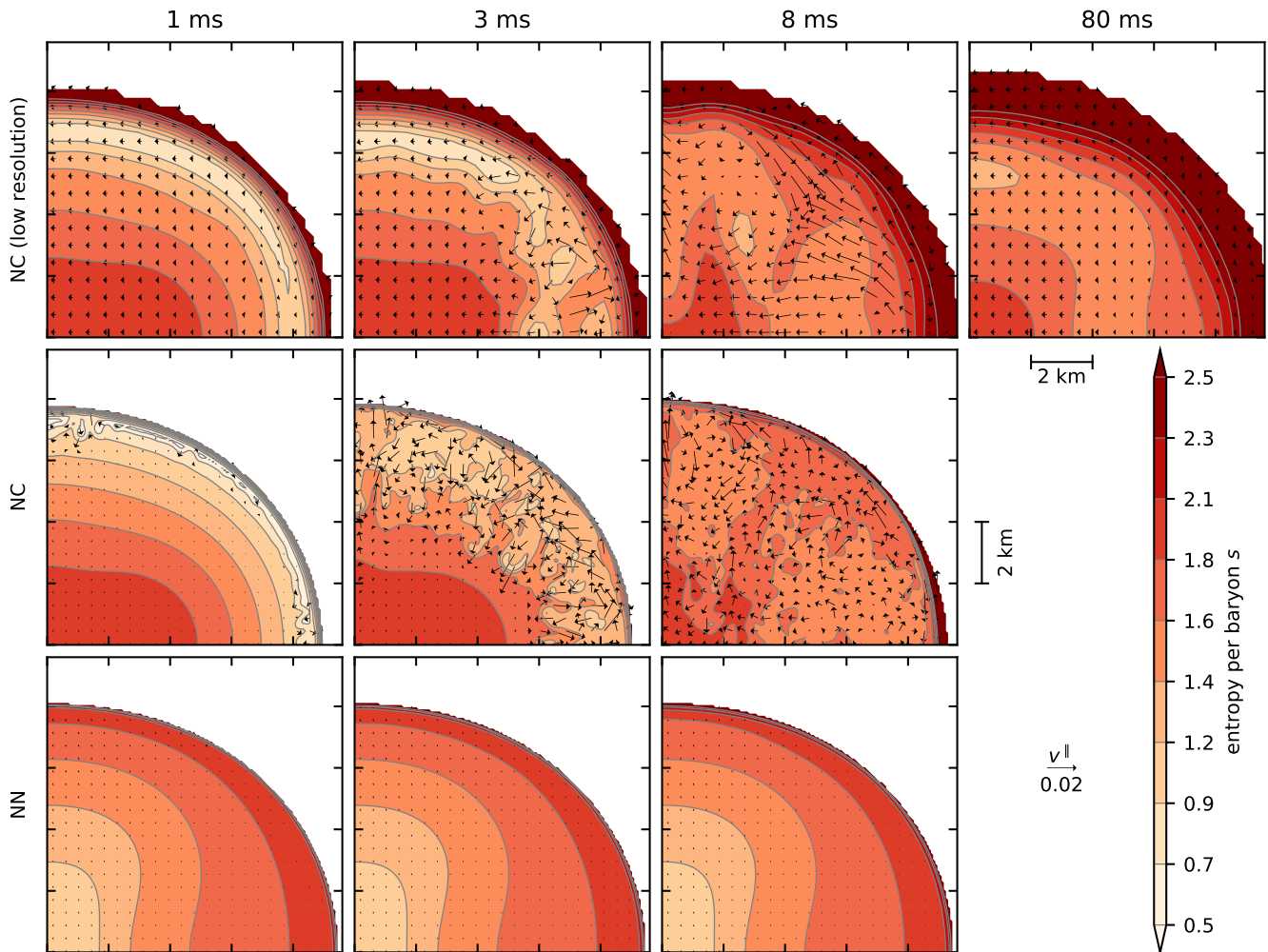


FIG. 9: Convection in the BAM evolution. Each row refers to a different stellar model and each column to a different time snapshot. The entropy per baryon s is shown as color filled contours and the parallel velocity $v^{\parallel} = v^r \mathbf{e}_r + rv^{\theta} \mathbf{e}_{\theta}$ as a vector field. See text for details.

and for barotropic stars in the case of s .

5. As already pointed out, the method we developed to obtain non-barotropic configurations does not depend on the XCFC approximation and can be easily adapted to the full stationary metric (even without the circularity assumption) or to Newtonian gravity (see Appendix A). All that is really needed to have non-barotropy is that the potential Q depends on more than just the pressure [e.g., $Q(p, x)$], that the second free variable x has a spatial distribution different from p , and that the cross partial derivative of the potential $\partial_p \partial_x Q$ is not null. In this paper we chose the second variable to be the angular velocity, $x = \Omega$, and we therefore consider differentially rotating neutron stars, but in principle we could as well have used the magnetic field or meridional currents [55] instead (or in addition).
6. It is known that the numerical solution of the Eu-

ler equation for a Newtonian non-barotropic star shows a degeneracy in the profile of Ω that can be lifted by e.g. including viscosity [24]. This degeneracy does not arise in our method because we fix the potential $Q(p, \Omega)$ and therefore we implicitly fix the profile of Ω .

Note that points 1 and 2 are a reformulation of the relativistic von Zeipel's theorem [56, 57].

B. General entropy profile

In principle, it is possible to use the formalism developed in this paper to determine the rotating profile of a hot neutron star given its 2D thermal profile $s = s(r, \theta)$.

Let us assume a potential that further generalizes

$Q(p, \Omega)$ in Eq. (38), for example

$$Q(p, \Omega) = \sum_{l,m} a_{lm} H^l(p) \mathcal{F}^m(\Omega), \quad (48)$$

where a_{lm} are parameters and H and \mathcal{F} are formally defined as before. Now, given a choice of a_{lm} , we obtain a unique profile $s(r, \theta)$ from the solution of Eqs. (35)–(37). To ensure that the entropy in a given point within the star takes a specified value, $s(r', \theta') = s'$, one can modify the potential free parameters, e.g., $a_{l'm'}$. If we want to fix the entropy in two points, we must tweak two free parameters, and so on. In principle we can fix the entropy in all grid points by adjusting an equal number of parameters.

In practice, the procedure described above may be cumbersome if one wants to fix the entropy in more than a few points and we discussed it only as a proof of principle. Moreover, this procedure works only for *planar* configurations, namely $s(r, \theta) = s(r, \pi - \theta)$. To obtain a non-planar configuration one should define two potentials Q_- and Q_+ that coincide together with their first and second partial derivatives along a given curve $(p(z), \Omega(z))$, where z is the curve parameter.

We remark that this procedure would work also if one wants to fix the rotational profile $\Omega = \Omega(r, \theta)$ instead of the entropy one.

C. Multi-dimensional equation of state

Let us consider an EOS that depends on $N > 2$ independent variables, e.g. $h = h(p, s, Y)$, where Y is the proton number fraction.

In this case one should solve Eqs. (35)–(36) as for the non-barotropic case of the EOS with two independent variables. The difference is that Eq. (37) now becomes

$$\partial_p Q(p, \Omega) = \frac{1}{\mathcal{L}(p, s(r, \theta), Y(r, \theta))}. \quad (49)$$

At this point, one can fix $Y(r, \theta)$ and invert the EOS to determine $s(r, \theta)$. Another way to look at this is that the 3D EOS is equivalent to a parameterized 2D EOS: $\mathcal{L}(p, s, Y(r, \theta)) = \mathcal{L}_{Y(r, \theta)}(p, s)$.

We remark that:

- It is possible to fix $s(r, \theta)$ instead of $Y(r, \theta)$, but not both profiles at the same time, unless one uses the procedure discussed in Sec. VIB.
- The results discussed above would stay valid when s and/or Y do not explicitly depend on (r, θ) but on (p, Ω) , since all these quantities are known when one solves Eq. (49).

D. Legendre transformation

In thermodynamics, different choices of free variables imply the use of different thermodynamical potentials,

that are related to each other by Legendre transformations. What if we take the Legendre transformation of the potential Q ?

First, we define the following transformed potential

$$\mathcal{Q}(p, F) = Q(p, \Omega(p, F)) - \Omega(p, F)F, \quad (50)$$

where the independent variables are p, F and therefore the angular velocity is written as $\Omega = \Omega(p, F)$, cf. Eq. (B12). The differential of Eq. (50) yields

$$d\mathcal{Q} = \frac{dp}{\mathcal{L}} - \Omega dF, \quad (51)$$

$$\mathcal{L}^{-1} = \left. \frac{\partial \mathcal{Q}}{\partial p} \right|_F, \quad (52)$$

$$\Omega = - \left. \frac{\partial \mathcal{Q}}{\partial F} \right|_p, \quad (53)$$

where all quantities depend on (p, F) .

In order to re-obtain the barotropic, differentially rotating model we assume that the EOS is an effective barotrope and that $\Omega = \Omega(F)$. Similarly to what was done in Sec. IIB, we can define a function $\mathcal{G} = \mathcal{G}(F)$ such that

$$\Omega(F) = - \frac{d\mathcal{G}(F)}{dF}. \quad (54)$$

The j -const differential-rotation law is equivalent to

$$\mathcal{G}(F) = \left(\frac{\sigma^2}{2} F - \Omega_0 \right) F, \quad (55)$$

where $\sigma = 1/R_0$ is a parameter. The barotropic potential of Eq. (38) is equivalent to the following barotropic transformed potential:

$$\mathcal{Q}(p, F) = H(p) + \mathcal{G}(F) - \ln \alpha_0. \quad (56)$$

An advantage of this formulation is that it unifies rigidly and differentially rotating stars. Indeed, the rigid rotation limit $R_0 \rightarrow \infty$ corresponds to $\sigma = 0$ and therefore $\Omega(F) \equiv \Omega_0$ is well defined. It also simplifies the inclusion of differential rotation laws where $F(\Omega)$ is not monotonic [32], which are a more realistic description of post-merged neutron stars.

VII. CONCLUSIONS

In this paper we have studied, for the first time, a stationary, differentially rotating, non-barotropic neutron star in General Relativity. In doing so, we have shown with theoretical arguments and with stationary and dynamical numerical simulations how the Euler equation can be cast in a potential form also in the non-barotropic case. This is a novel results even in the context of Newtonian stars.

To test our approach, we have first generated stationary configurations using the XNS code [14–16], that determines the neutron star structure and spacetime in

the eXtended Conformal Flatness Condition approximation [35]. We have then taken the stationary configurations as initial condition for dynamical evolutions performed with the general relativistic hydrodynamics code BAM [40, 41]. We considered consistently determined configurations of barotropic and non-barotropic rotating neutron stars and compared them with non-consistent “control” configuration to gauge the quality of our models. We considered both convectively stable and unstable models.

We used our formalism to demonstrate some properties of non-barotropic stars, most notably that a non-barotropic star must be differentially rotating [56, 57] and that in a non-barotropic star the specific angular momentum and the entropy must depend on both pressure and angular velocity.

Possible outlooks of this work are the following.

One can use the final snapshots of dynamical evolutions to model the Euler equation potential of (i) post merged neutron stars, (ii) proto neutron stars (post core collapse), and (iii) post hadron phase transition quark stars. Then, one can quickly explore the parameter space of the hot rotating remnant with a stationary code like XNS to study e.g. the dynamical stability, the maximal mass, the gravitational wave signal from stellar quasi-periodic oscillations, etc. The most interesting configurations can then be selected to be further explored with dynamical codes like BAM, using the XNS output as completely consistent initial data [e.g., 16].

In Sec. VIB we showed how in principle is possible to use our potential formalism to determine a general entropy profile. But another, maybe simpler, method would be to import the techniques developed in the context of Newtonian baroclinic stars to include a general thermal profile. In this way one can study the long term (on the order of minutes), neutrino-driven, quasi-stationary evolution of the hot and rotating remnant of cases (i–iii) [34, 58–62]. This is important because a huge amount of energy (up to tenths of solar masses) is expected to be radiated through neutrinos in the first phase of the neutron star life. However, this phase is too long to be fully explored with dynamical codes, while using a quasi-stationary evolution would allow to employ stationary, fast codes like XNS. Again, in this way one can quickly study the parameter space and select the most interesting configurations to be further explored with dynamical codes, and even study the time dependent gravitational wave signal from this phase [63, 64] and assess the role of physical processes such as viscosity.

Finally, one can apply our potential formalism to the study of non-barotropicity in accretion disks [27, 28, 33], in neutron stars with magnetic field [65] and with meridional currents [55], and in Newtonian stars.

Appendix A: Newtonian limit

In the Newtonian limit,

$$\alpha \rightarrow \exp \Phi, \quad (\text{A1})$$

$$\ell \rightarrow \rho, \quad (\text{A2})$$

$$R \rightarrow \varpi = r \sin \theta, \quad (\text{A3})$$

$$v^\phi \rightarrow \Omega, \quad (\text{A4})$$

$$F \rightarrow j = \varpi^2 \Omega, \quad (\text{A5})$$

$$\ell \rightarrow j = \varpi^2 \Omega, \quad (\text{A6})$$

$$Q \rightarrow - \left(\Phi - \frac{1}{2} \varpi^2 \Omega^2 \right), \quad (\text{A7})$$

where Φ is the gravitational potential, ϖ the cylindrical radius, and j the non-relativistic specific angular momentum. Note that both F and ℓ tend to the same limit: j , and that the potential Q [Eq. (29)] tends to minus the effective (including the centrifugal force) gravitational potential. The Newtonian limit of Eq. (4) is:

$$\frac{\nabla p}{\rho} + \nabla \left(\Phi - \frac{1}{2} \varpi^2 \Omega^2 \right) + j \nabla \Omega = 0, \quad (\text{A8})$$

where $i = \{r, \theta\}$ and we divided by r the equation along the θ direction.

Eq. (A8) is equivalent to the stationary Euler equation adopted in the Newtonian literature, [e.g., Eqs. (2)–(3) of Ref. 21 and Eq. (20) of Ref. 24]

$$\frac{\nabla p}{\rho} + \nabla \Phi - \varpi \Omega^2 \mathbf{e}_\varpi = 0, \quad (\text{A9})$$

where \mathbf{e}_ϖ is a unit vector along the cylindrical radius and we assumed circular motion (i.e., no meridional currents) and no viscosity.

We will show here that Eqs. (A8)–(A9) are equivalent by recovering both from the general form of the stationary (Newtonian) Euler equation:

$$(\mathbf{v} \cdot \nabla) \mathbf{v} = - \frac{\nabla p}{\rho} - \nabla \Phi, \quad (\text{A10})$$

where $\mathbf{v} = \Omega \varpi \mathbf{e}_\phi$ is the fluid velocity. From the identity

$$(\mathbf{v} \cdot \nabla) \mathbf{v} = \frac{1}{2} \nabla (\mathbf{v} \cdot \mathbf{v}) - \mathbf{v} \times (\nabla \times \mathbf{v}), \quad (\text{A11})$$

we get

$$(\mathbf{v} \cdot \nabla) \mathbf{v} = \frac{1}{2} \nabla (\varpi^2 \Omega^2) - x, \quad (\text{A12})$$

$$x = \Omega \sin \theta \partial_r (r \varpi \Omega) \mathbf{e}_r + \Omega \partial_\theta (\sin \theta \varpi \Omega) \mathbf{e}_\theta. \quad (\text{A13})$$

Now, if we directly expand the partial derivatives in x ,

$$x = \left(\mathbf{e}_r \partial_r + \frac{\mathbf{e}_\theta}{r} \partial_\theta \right) \frac{\varpi^2 \Omega^2}{2} + \varpi \Omega^2 (\sin \theta \mathbf{e}_r + \cos \theta \mathbf{e}_\theta), \quad (\text{A14})$$

we recover Eq. (A9).

On the other hand, we have also

$$x = \Omega \partial_r (\varpi^2 \Omega) \mathbf{e}_r + \frac{\Omega}{r} \partial_\theta (\varpi^2 \Omega) \mathbf{e}_\theta \\ = \nabla (\varpi^2 \Omega^2) - \varpi^2 \Omega \nabla \Omega, \quad (\text{A15})$$

from which we recover Eq. (A8).

Our non-barotropic potential formalism can be simply extended to the Newtonian case by applying it to Eq. (A8).

Appendix B: 2D equation of state

We choose a polytropic expression for the total energy per baryon:

$$e(\rho, s) = m_n (1 + u_{\text{cold}}(\rho) + u_{\text{th}}(\rho, s)), \quad (\text{B1})$$

$$u_{\text{cold}}(\rho) = k_1 \rho^{\Gamma-1}, \quad (\text{B2})$$

$$u_{\text{th}}(\rho, s) = k_2 s^2 \rho^{\Gamma_{\text{th}}-1}, \quad (\text{B3})$$

where ρ is the rest mass density, s the entropy per baryon, m_n is the nucleon mass, u_{cold} the specific cold internal energy, u_{th} the specific thermal internal energy, and k_1, Γ, k_2 and Γ_{th} are parameters. We remark that to have physical results for any physical ρ, s it has to be $\Gamma > 1, \Gamma_{\text{th}} > 1, k_1 > 0$, and $k_2 \geq 0$. Using the relation (that is a consequence of the first law of Thermodynamics)

$$\frac{p}{\rho^2} = \frac{1}{m_n} \left. \frac{\partial e}{\partial \rho} \right|_s, \quad (\text{B4})$$

where p is the pressure, we get

$$p(\rho, s) = (\Gamma - 1) \rho u_{\text{cold}}(\rho) + (\Gamma_{\text{th}} - 1) \rho u_{\text{th}}(\rho, s). \quad (\text{B5})$$

Eq. (B5) can be written as

$$p(\rho, u_{\text{th}}) = K \rho^\Gamma + (\Gamma_{\text{th}} - 1) \rho u_{\text{th}}, \quad (\text{B6})$$

$$K = (\Gamma - 1) k_1, \quad (\text{B7})$$

namely we recover Eq. (44).

Using the thermodynamical relation

$$T = \left. \frac{\partial e}{\partial s} \right|_\rho, \quad (\text{B8})$$

where T is the temperature, we obtain

$$T(\rho, s) = 2 m_n k_2 s \rho^{\Gamma_{\text{th}}-1}. \quad (\text{B9})$$

We remark that $T \rightarrow 0$ as $s \rightarrow 0$, as expected.

The speed of sound is defined by

$$c_s = \sqrt{\left. \frac{\partial p}{\partial \epsilon} \right|_s}, \quad (\text{B10})$$

where $\epsilon = \rho e / m_n$ is the total energy density. For our EOS it is

$$c_s^2 = \frac{\Gamma(\Gamma - 1) k_1 \rho^\Gamma + \Gamma_{\text{th}} (\Gamma_{\text{th}} - 1) s^2 k_2 \rho^{\Gamma_{\text{th}}}}{\rho + \Gamma k_1 \rho^\Gamma + \Gamma_{\text{th}} s^2 k_2 \rho^{\Gamma_{\text{th}}}}. \quad (\text{B11})$$

From the Legendre transformation of the specific energy

$$h(p, s) = \frac{e(\rho(p, s), s)}{m_n} + \frac{p}{\rho(p, s)}, \quad (\text{B12})$$

we get the specific enthalpy h

$$h(p, s) = 1 + \Gamma k_1 (\rho(p, s))^{\Gamma-1} \\ + \Gamma_{\text{th}} k_2 s^2 (\rho(p, s))^{\Gamma_{\text{th}}-1}, \quad (\text{B13})$$

where $\rho(p, s)$ is the inverse of Eq. (B5). The reason why we write all quantities in terms of p and s is that h is naturally a function of these variables, see discussion in Sec. II A.

From the solution of the Euler equation [Eqs. (35)-(37)] we obtain \mathcal{L} and p , from which we want to get all the other thermodynamical quantities. To invert the EOS, we first cancel out the term with the entropy and obtain the equation

$$(\Gamma_{\text{th}} - 1) \mathcal{L} - \Gamma_{\text{th}} p = (\Gamma_{\text{th}} - 1) \rho + (\Gamma_{\text{th}} - \Gamma) k_1 \rho^\Gamma, \quad (\text{B14})$$

where $\mathcal{L} = h \rho$ is the enthalpy density and the only unknown is the density ρ . This equation can be easily solved if $\Gamma = 3/2$ (when it becomes cubic in $\sqrt{\rho}$), $\Gamma = 2$ (quadratic in ρ) or $\Gamma = 3$ (cubic in ρ).

We pick $\Gamma = 3$ because it is closer to the stiffness expected for the high-density part of the real EOS [66]. We can at this point set the parameter k_1 enforcing the condition $2.1 \lesssim M_{\text{max}} \lesssim 3$, where M_{max} is the maximal non-rotating mass.

We choose $\Gamma_{\text{th}} = 1.75$, which is a value that reproduces the behavior of known finite-temperature EOSs [67, 68]. To set k_2 we require that the thermal contribution to the pressure at $\rho = 2\rho_n$ and $s = 2k_B$ is approximately 30%, value determined by inspection of realistic EOSs. The corresponding temperature is $T(2\rho_n, 2k_B) \simeq 29 \text{ MeV}/k_B$.

The solution of Eq. (B14) is not always unique. In particular, when $\Gamma_{\text{th}} < \Gamma = 3$ there are values of (\mathcal{L}, p) which correspond to two valid solutions (ρ_1, s_1) and (ρ_2, s_2) with $\rho_1 \leq \rho_c \leq \rho_2$, where ρ_c is a critical density that depends on $\Gamma, \Gamma_{\text{th}}, k_1$:

$$\rho_c = \sqrt{\frac{\Gamma_{\text{th}} - 1}{3k_1(\Gamma - \Gamma_{\text{th}})}} \quad (\Gamma_{\text{th}} < \Gamma = 3). \quad (\text{B15})$$

A way around this difficulty is to choose a stellar configuration such that the maximal density is lower than ρ_c , in order to safely take the root ρ_1 .

We report the EOS parameters in Table II. With those, we get the following EOS properties (cf. Fig. 5):

- Critical density for EOS inversion: $\rho_c = 4.61\rho_n$.
- The speed of sound of the cold EOS becomes greater than the speed of light at $\rho_{c_s} = 5.95\rho_n$.
- Central density of the (cold, non-rotating) maximal mass configuration: $\rho_{\max} = 6.90\rho_n$.
- Maximal mass of the cold, non-rotating star: $M_{\max} = 2.22 M_\odot$,

where ρ_{\max} and M_{\max} are obtained enforcing causality at densities greater than ρ_{c_s} and without attaching a crust at low densities.

Since all considered models have a central density $\rho_0 = 4\rho_n$ (see Table II), we avoid the problems related to causality and uniqueness. This value is also smaller than the central density ρ_{\max} of the non-rotating maximal mass configuration; and since additionally we chose Ω_0 such that the gravitational (Komar) mass is smaller than (but close to) the maximal non-rotating mass, then all studied models are dynamically stable (i.e., they do not collapse).

Appendix C: Barotropic EOS

When the EOS is an effective barotrope every thermodynamical quantity depends only on the pressure, for example $s = \tilde{s}(p)$, $\rho = \tilde{\rho}(p)$, $h = \tilde{h}(p)$, ... (we mark the barotropic functions with a tilde to stress that they correspond to physical quantities only in a barotropic stellar model, while the pressure p is always equivalent to the physical quantity).

The easiest choice for the barotropic function is

$$\tilde{s}(p) = k_3(\tilde{\rho}(p))^{\frac{\Gamma - \Gamma_{\text{th}}}{2}}, \quad (\text{C1})$$

where k_3 is a constant; in this case the heat integral can be easily integrated in $\tilde{\rho}$:

$$H(p) = \int_{\tilde{\rho}(p_0)}^{\tilde{\rho}(p)} \frac{p'(\tilde{\rho})}{\tilde{\mathcal{L}}(p(\tilde{\rho}))} d\tilde{\rho}, \quad (\text{C2})$$

where p_0 is the central pressure, $\tilde{\mathcal{L}}$ is the enthalpy density, $p(\tilde{\rho})$ is the inverse of $\tilde{\rho}(p)$, and $p'(\tilde{\rho})$ is its total derivative with respect to $\tilde{\rho}$. Indeed, in this case we analytically obtain

$$H(p) = \frac{\Gamma[(\Gamma - 1)k_1 + (\Gamma_{\text{th}} - 1)k_2k_3^2]}{(\Gamma - 1)[\Gamma k_1 + \Gamma_{\text{th}}k_2k_3^2]} \ln \frac{\tilde{h}(p)}{\tilde{h}_0}. \quad (\text{C3})$$

where \tilde{h}_0 is the central specific enthalpy. We remark that $H = \ln h/h_0$ when $k_2k_3^2 = 0$ (i.e., cold star) or $\Gamma = \Gamma_{\text{th}}$ (i.e., isentropic star), as it should be.

We will consider another possibility for the barotropic function:

$$\tilde{s}(p) = \tilde{s}_s - k_3\tilde{\rho}(p), \quad (\text{C4})$$

where \tilde{s}_s is the surface entropy and k_3 a constant. Unfortunately in this case there is no simple analytical form for the heat integral and we integrate Eq. (C2) numerically.

Let us now consider the stability of the star against convection. We will use the convective criterion in spherical symmetry, namely for a non-rotating neutron star, as an estimate for our rotating case. In spherical symmetry the star is unstable against convection when the Schwarzschild discriminant is negative [69],

$$S(\bar{r}) = \frac{dp}{d\bar{r}} - c_s^2 \frac{d\epsilon}{d\bar{r}} < 0, \quad (\text{C5})$$

where c_s is the speed of sound [Eq. (B11)] and the total derivatives are taken along the Schwarzschild radius \bar{r} that is related to the isotropic radius by

$$\frac{d\bar{r}}{\sqrt{\bar{r}^2 - 2m(\bar{r})\bar{r}}} = \frac{dr}{r}, \quad (\text{C6})$$

where $m(\bar{r})$ is the gravitational mass enclosed in \bar{r} .

For our EOS, Eq. (C5) is equivalent to

$$[(\Gamma_{\text{th}} - 1) + k_1\Gamma(\Gamma_{\text{th}} - \Gamma)\rho^{\Gamma-1}] \frac{ds}{d\bar{r}} < 0. \quad (\text{C7})$$

For our choice of $\Gamma_{\text{th}} < \Gamma$, this means that if the entropy gradient is negative (resp. positive) there is convection when $\rho < \rho_c$ (resp. $\rho > \rho_c$), where the critical density for convection ρ_c happens to be equal to the critical density for inverting the EOS, Eq. (B15). Then, since in our models the rest mass density is always smaller than ρ_c , we expect convection for barotropic profiles given by Eq. (C1) and vice versa no convection for barotropic profiles given by Eq. (C4).

For the case with convection, the convective timescale is given by the analytical estimate [69] (g is the strength of the gravity acceleration)

$$\tau_c = c_s \sqrt{\frac{2\mathcal{L}}{-gS(\bar{r})}}, \quad (\text{C8})$$

which is of the order of tens of milliseconds close to the stellar center and reduces to a timescale of the order of 0.1 ms close to the stellar surface (these timescales are compatible with those found by De Pietri et al. [70] and De Pietri et al. [71] in their simulations). This means that we expect convection to influence our dynamical simulations (that last for 10 ms), and that it starts at the surface and propagates to the center.

While this analysis is strictly valid only for a non-rotating barotropic star, we find that its application to rotating non-barotropic stars qualitatively agrees with the results obtained from dynamical simulations [Sec. V].

Acknowledgments

TD acknowledges support by the European Union's Horizon 2020 research and innovation program under

grant agreement No 749145, BNSmergers. SR has been supported by the Swedish Research Council (VR) under grant number 2016-03657 3, by the Swedish National Space Board under grant number Dnr. 107/16 and by the VR research environment grant Gravitational Radiation and Electromagnetic Astrophysical Transients (GREAT) under Dnr. 2016-06012. Support from the COST Actions

on neutron stars (PHAROS; CA16214) and black holes and gravitational waves (GWerse; CA16104) are gratefully acknowledged.

We are grateful to M.A. Abramowicz, B. Brügmann, S. Faraji, C. Lundman, J.A. Pons, and M. Rieutord for useful discussions and comments on the paper draft.

-
- [1] J. M. Lattimer, *Ann. Rev. Nucl. Part. Sci.* **62**, 485 (2012), 1305.3510.
- [2] J. M. Lattimer and M. Prakash, *Phys. Rept.* **621**, 127 (2016), 1512.07820.
- [3] B. P. Abbott et al. (LIGO Scientific, Virgo), *Phys. Rev. Lett.* **121**, 161101 (2018), 1805.11581.
- [4] A. Perego, S. Bernuzzi, and D. Radice, *Eur. Phys. J.* **A55**, 124 (2019), 1903.07898.
- [5] T. Fischer, I. Sagert, G. Pagliara, M. Hempel, J. Schaffner-Bielich, T. Rauscher, F. K. Thielemann, R. Käppeli, G. Martínez-Pinedo, and M. Liebendörfer, *The Astrophysical Journal Supplement Series* **194**, 39 (2011), 1011.3409.
- [6] M. Punturo et al., *Class. Quant. Grav.* **27**, 194002 (2010).
- [7] B. S. Sathyaprakash et al. (2019), 1903.09221.
- [8] B. P. Abbott, R. Abbott, T. D. Abbott, F. Acernese, K. Ackley, C. Adams, T. Adams, P. Addesso, R. X. Adhikari, V. B. Adya, et al., *Physical Review Letters* **119**, 161101 (2017), 1710.05832.
- [9] B. P. Abbott, R. Abbott, T. D. Abbott, F. Acernese, K. Ackley, C. Adams, T. Adams, P. Addesso, R. X. Adhikari, V. B. Adya, et al., *Astrophys. J. Lett.* **848**, L12 (2017), 1710.05833.
- [10] D. A. Coulter, R. J. Foley, C. D. Kilpatrick, M. R. Drout, A. L. Piro, B. J. Shappee, M. R. Siebert, J. D. Simon, N. Ulloa, D. Kasen, et al., *Science* **358**, 1556 (2017), 1710.05452.
- [11] A. Burrows, *Astrophys. J.* **334**, 891 (1988).
- [12] S. Bonazzola, E. Gourgoulhon, M. Salgado, and J. A. Marck, *Astron. Astrophys.* **278**, 421 (1993).
- [13] J. O. Goussard, P. Haensel, and J. L. Zdunik, *Astron. Astrophys.* **321**, 822 (1997), astro-ph/9610265.
- [14] N. Bucciantini and L. Del Zanna, *Astron. Astrophys.* **528**, A101 (2011), 1010.3532.
- [15] A. G. Pili, N. Bucciantini, and L. Del Zanna, *Mon. Not. R. Astron. Soc.* **439**, 3541 (2014), 1401.4308.
- [16] G. Camelio, T. Dietrich, and S. Rosswog, *Mon. Not. R. Astron. Soc.* **480**, 5272 (2018), 1806.07775.
- [17] I. W. Roxburgh and P. A. Strittmatter, *Mon. Not. R. Astron. Soc.* **133**, 345 (1966).
- [18] M. J. Clement, *Astrophys. J.* **156**, 1051 (1969).
- [19] J. J. Monaghan, *Mon. Not. R. Astron. Soc.* **154**, 47 (1971).
- [20] C. M. Sharp, R. C. Smith, and D. L. Moss, *Mon. Not. R. Astron. Soc.* **179**, 699 (1977).
- [21] K. Uryu and Y. Eriguchi, *Mon. Not. R. Astron. Soc.* **269**, 24 (1994).
- [22] I. W. Roxburgh, *Astron. Astrophys.* **454**, 883 (2006).
- [23] F. Espinosa Lara and M. Rieutord, *Astron. Astrophys.* **470**, 1013 (2007).
- [24] F. Espinosa Lara and M. Rieutord, *Astron. Astrophys.* **552**, A35 (2013), 1212.0778.
- [25] N. Yasutake, K. Fujisawa, and S. Yamada, *Mon. Not. R. Astron. Soc.* **446**, L56 (2015), 1402.4567.
- [26] K. Fujisawa, *Mon. Not. R. Astron. Soc.* **454**, 3060 (2015), 1507.02693.
- [27] P. Amendt, A. Lanza, and M. A. Abramowicz, *The Astrophysical Journal* **343**, 437 (1989).
- [28] D. N. Razdoburdin, *Astronomische Nachrichten* **338**, 799 (2017), 1708.08716.
- [29] J. M. Bardeen, *The Astrophysical Journal* **162**, 71 (1970).
- [30] N. Stergioulas, *Living Reviews in Relativity* **6**, 3 (2003), ISSN 1433-8351, URL <https://doi.org/10.12942/lrr-2003-3>.
- [31] H. Komatsu, Y. Eriguchi, and I. Hachisu, *Mon. Not. R. Astron. Soc.* **237**, 355 (1989).
- [32] K. Uryū, A. Tsokaros, L. Baiotti, F. Galeazzi, K. Taniguchi, and S. Yoshida, *Phys. Rev. D* **96**, 103011 (2017), 1709.02643.
- [33] V. Witzany and P. Jofre, *614*, A75 (2019), ISSN 0004-6361, 1432-0746, URL <https://www.aanda.org/articles/aa/abs/2018/06/aa32361-17/aa32361-17.html>.
- [34] L. Villain, J. A. Pons, P. Cerdá-Durán, and E. Gourgoulhon, *Astron. Astrophys.* **418**, 283 (2004), astro-ph/0310875.
- [35] I. Cordero-Carrión, P. Cerdá-Durán, H. Dimmelmeier, J. L. Jaramillo, J. Novak, and E. Gourgoulhon, *Phys. Rev. D* **79**, 024017 (2009), 0809.2325.
- [36] E. Gourgoulhon, arXiv e-prints arXiv:1003.5015 (2010), 1003.5015.
- [37] P. Iosif and N. Stergioulas, *General Relativity and Gravitation* **46**, 1800 (2014), 1406.7375.
- [38] N. Stergioulas and J. L. Friedman, *Astrophys. J.* **444**, 306 (1995), astro-ph/9411032.
- [39] B. Brügmann, W. Tichy, and N. Jansen, *Phys. Rev. Lett.* **92**, 211101 (2004), gr-qc/0312112.
- [40] B. Brügmann, J. A. Gonzalez, M. Hannam, S. Husa, U. Sperhake, et al., *Phys. Rev. D* **77**, 024027 (2008), gr-qc/0610128.
- [41] M. Thierfelder, S. Bernuzzi, and B. Brügmann, *Phys. Rev. D* **84**, 044012 (2011), 1104.4751.
- [42] T. Dietrich, S. Bernuzzi, M. Ujevic, and B. Brügmann, *Phys. Rev. D* **91**, 124041 (2015), 1504.01266.
- [43] S. Bernuzzi and T. Dietrich, *Phys. Rev. D* **94**, 064062 (2016), 1604.07999.
- [44] T. Dietrich, S. Ossokine, and K. Clough, *Class. Quant. Grav.* **36**, 025002 (2019), 1807.06959.
- [45] S. Bernuzzi and D. Hilditch, *Phys. Rev. D* **81**, 084003 (2010), 0912.2920.
- [46] A. Weyhausen, S. Bernuzzi, and D. Hilditch, *Phys. Rev. D* **85**, 024038 (2012), 1107.5539.
- [47] D. Hilditch, S. Bernuzzi, M. Thierfelder, Z. Cao,

- W. Tichy, et al., Phys. Rev. **D88**, 084057 (2013), 1212.2901.
- [48] R. Borges, M. Carmona, B. Costa, and W. S. Don, Journal of Computational Physics **227**, 3191 (2008), ISSN 0021-9991, URL <http://www.sciencedirect.com/science/article/pii/S0021999107005232>.
- [49] S. Bernuzzi, M. Thierfelder, and B. Bruegmann, Phys. Rev. **D85**, 104030 (2012), 1109.3611.
- [50] T. Dietrich, S. Bernuzzi, B. Bruegmann, and W. Tichy, in *Proceedings, 26th Euromicro International Conference on Parallel, Distributed and Network-based Processing (PDP 2018): Cambridge, UK, March 21-23, 2018* (2018), pp. 682–689, 1803.07965.
- [51] T. Dietrich, D. Radice, S. Bernuzzi, F. Zappa, A. Perego, B. Brgmann, S. V. Chaurasia, R. Dudi, W. Tichy, and M. Ujevic, Class. Quant. Grav. **35**, 24LT01 (2018), 1806.01625.
- [52] T. Dietrich, A. Samajdar, S. Khan, N. K. Johnson-McDaniel, R. Dudi, and W. Tichy (2019), 1905.06011.
- [53] K. Kiuchi, K. Kawaguchi, K. Kyutoku, Y. Sekiguchi, M. Shibata, and K. Taniguchi, Phys. Rev. **D96**, 084060 (2017), 1708.08926.
- [54] F. Guercilena, D. Radice, and L. Rezzolla, Comput. Astrophys. Cosmol. **4**, 3 (2017), 1612.06251.
- [55] R. Birkel, N. Stergioulas, and E. Müller, Phys. Rev. D **84**, 023003 (2011), 1011.5475.
- [56] H. v. Zeipel, Monthly Notices of the Royal Astronomical Society **84**, 665 (1924), ISSN 0035-8711, <http://oup.prod.sis.lan/mnras/article-pdf/84/9/665/2793230/mnras84-0665.pdf>, URL <https://doi.org/10.1093/mnras/84.9.665>.
- [57] M. A. Abramowicz, Acta Astron. **21**, 81 (1971).
- [58] A. Burrows and J. M. Lattimer, Astrophys. J. **307**, 178 (1986).
- [59] W. Keil and H. T. Janka, Astron. Astrophys. **296**, 145 (1995).
- [60] J. A. Pons, S. Reddy, M. Prakash, J. M. Lattimer, and J. A. Miralles, Astrophys. J. **513**, 780 (1999), astro-ph/9807040.
- [61] L. F. Roberts, The Astrophysical Journal **755**, 126 (2012), URL <https://doi.org/10.1088%2F0004-637x%2F755%2F2%2F126>.
- [62] G. Camelió, L. Gualtieri, J. A. Pons, and V. Ferrari, Phys. Rev. D **94**, 024008 (2016), 1601.02945.
- [63] V. Ferrari, G. Miniutti, and J. A. Pons, Monthly Notices of the Royal Astronomical Society **342**, 629 (2003), ISSN 0035-8711, <http://oup.prod.sis.lan/mnras/article-pdf/342/2/629/3433686/342-2-629.pdf>, URL <https://doi.org/10.1046/j.1365-8711.2003.06580.x>.
- [64] G. Camelió, A. Lovato, L. Gualtieri, O. Benhar, J. A. Pons, and V. Ferrari, Phys. Rev. D **96**, 043015 (2017), 1704.01923.
- [65] D. Chatterjee, T. Elghozi, J. Novak, and M. Oertel, Monthly Notices of the Royal Astronomical Society **447**, 3785 (2015), ISSN 0035-8711, <http://oup.prod.sis.lan/mnras/article-pdf/447/4/3785/5792844/stu2706.pdf>, URL <https://doi.org/10.1093/mnras/stu2706>.
- [66] S. Rosswog and M. B. Davies, Monthly Notices of the Royal Astronomical Society **334**, 481 (2002), astro-ph/0110180.
- [67] A. Bauswein, H.-T. Janka, and R. Oechslin, Phys. Rev. D **82**, 084043 (2010), URL <https://link.aps.org/doi/10.1103/PhysRevD.82.084043>.
- [68] H. Yasin, S. Schäfer, A. Arcones, and A. Schwenk, arXiv e-prints arXiv:1812.02002 (2018), 1812.02002.
- [69] K. S. Thorne, Astrophys. J. **144**, 201 (1966).
- [70] R. De Pietri, A. Feo, J. A. Font, F. Löffler, F. Maione, M. Pasquali, and N. Stergioulas, Phys. Rev. Lett. **120**, 221101 (2018), URL <https://link.aps.org/doi/10.1103/PhysRevLett.120.221101>.
- [71] R. De Pietri, A. Feo, J. A. Font, F. Löffler, M. Pasquali, and N. Stergioulas, arXiv e-prints arXiv:1910.04036 (2019), 1910.04036.